Under Seawater Capacitive Power Transfer for Maritime Charging Applications

1st Hussein Mahdi
Department of Electrical Engineering
UiT - The Arctic University of Norway
Narvik, 8514, Norway
hussein.al-sallami@uit.no

2nd Reiji Hattori
Department of Applied Science
for Electronics and Materials (ASEM)
Kyushu University
Fukuoka, 816-8580 Japan
hattori@gic.kyushu-u.ac.jp

3rd Bjarte Hoff
Department of Electrical Engineering
UiT - The Arctic University of Norway
Narvik, 8514, Norway
bjarte.hoff@uit.no

4th Trond Østrem
Department of Electrical Engineering
UiT - The Arctic University of Norway
Narvik, Norway
trond.ostrem@uit.no

***Abstract*—Underwater capacitive power transfer (CPT) can provide an inexpensive and light electric charging solution with good misalignment tolerance for unmanned maritime vehicles. This paper investigates the effect of the changing of the frequency and the distance on the power transfer and overall efficiency of the underwater CPT system, considering the dielectric losses of the medium. It also proposes and validates a mathematical model for calculating the maximum available efficiency of the system. Using series compensations, the proposed CPT can transfer 48 W at 500 mm, 48 V input voltage, 516 kHz, and 54%.**

***Index Terms*—Underwater structures, marine vehicles, wireless charging, capacitive power transfer, maximum efficiency**

I. Introduction

Unmanned maritime vehicles (UMVs) have attracted considerable attention in recording oceanographic observations, studying climate change, and observing marine pollution. They can operate autonomously in challenging and hazardous shallow or deep water [1]. Both surface and underwater UMVs have been extensively used in marine exploitation investigation and emergency search rescue [2], [3]. Powered by lithium-ion batteries, these vehicles profile up hundreds to thousands of kilometers of the ocean vertically or horizontally under remote control over months [4].

Charging infrastructure can play a critical role in the development of battery-powered autonomous UMVs. Battery-swapping, wired charging, and wireless charging are three main charging approaches that can be adapted for charging maritime vehicles. Batteries swapping is time-consuming and requires human intervention, which losing their autonomy. Wired charging techniques are another approach that can be achieved manually or automatically. Automatically, various robotic docking and latching mechanism are proposed for both unmanned surface vehicles (USVs) [5] and autonomous underwater vehicles (AUVs) [6]. However, these techniques require high-precision connection mechanisms, which increase the design complexity and overall price of the system [7].

Wireless power transfer (WPT) technologies can provide autonomous charging without mechanical contact between the power source and maritime vehicles or ships. Inductive power transfer (IPT) is one of the WPT technologies that uses inductive coupling to wirelessly charge AUVs [8]–[11]. However, the proposed IPT systems can transfer power over a distance range of tens of millimeters to reduce the underwater eddy current losses. Besides, the systems comprise heavy, expensive, and fragile parts. Capacitive power transfer (CPT) is another WPT technology that utilizes electric fields to transfer power. It is an inexpensive and light charging solution with good misalignment tolerance.

Tamura et al. [12], [13] proposed underwater CPT systems for charging USVs. In [12], they transferred $400\,\mathrm{W}$ power under freshwater over $20\,\mathrm{mm}$ distance at $10.77\,\mathrm{MHz}$ and ac-ac efficiency exceeding 90%. While in [13], they designed under seawater CPT system that can transfer data and $100\,\mathrm{W}$ power under freshwater over $20\,\mathrm{mm}$ distance at $6.78\,\mathrm{MHz}$ and ac-ac efficiency exceeding 90%. Operating at a high-frequency range increases the complexity of the design and increases the losses at wide separation distances.

This paper will investigate the effect of the changing of the frequency and the distance on the power transfer and overall efficiency of the under seawater CPT system, considering the dielectric losses of the medium. It will also examine the horizontal and vertical four-plate structure to improve the system's transferability and efficiency. The rest of the paper is organized as follows: Section II introduces simple optimization criteria using a two-port approach to achieve maximum power transfer efficiency. Section III presents the experimental results. Finally, Section IV concludes the work.

II. Modeling Approach

The two-port network is a general formulation for the CPT scheme in which the capacitive couplers can be modeled as a black box from which only the voltages (u_1, u_2) and the

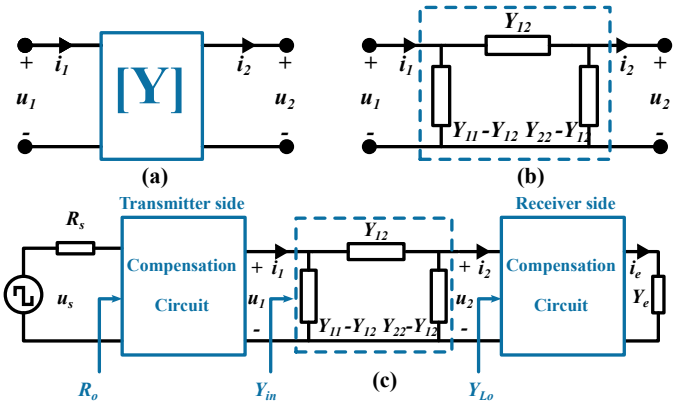

Fig. 1. The two-port network model of CPT system.

currents (i_1, i_2) can be measured, as shown in Fig. 1(a). The two-port network comprises the capacitive coupling parameters, which can be modeled using the conventional CPT π-network model, as illustrated in Fig. 1(b). The relationship between the input current and voltage to the output current and voltage can be expressed as

$$\begin{bmatrix} u_1 \\ i_1 \end{bmatrix} = \begin{bmatrix} A & B \\ C & D \end{bmatrix} \begin{bmatrix} u_2 \\ i_2 \end{bmatrix} = \begin{bmatrix} \frac{Y_{22}}{Y_{12}} & \frac{1}{Y_{12}} \\ \frac{Y_{11}Y_{22}-Y_{12}^2}{Y_{12}} & \frac{Y_{11}}{Y_{12}} \end{bmatrix} \begin{bmatrix} u_2 \\ i_2 \end{bmatrix} \tag{1}$$

This mathematical representation is more convenient when the capacitive two-port network is cascaded with other networks, such as the compensation circuits, as shown in Fig. 1(c). The determinant of the matrix is unity. For a lossless CPT system (i.e., the dielectric medium between the couplers is lossless), A and D are purely real, while B and C are pure imaginary values. If the CPT system is symmetric (i.e., $Y_{11} = Y_{22}$), then $A = D$.

In Fig. 1(c), the source resistor R_s represents the sum of the turn-on resistance of the switches in the inverter and the losses in the compensation circuit of the transmitter side. The resistor R_0 represents the overall resistance of the CPT system seen by the source. The parameter Y_in represents the admittance at the transmitter side, while the Y_out is the admittance at the receiver side. Finally, the Y_e represents the effective admittance of the load seen from the input of a rectifier. The input and output admittances can be expressed as

$$Y_\mathrm{in} = Y_{11} - \frac{Y_{12}^2}{Y_{22} + Y_\mathrm{Lo}} \tag{2}$$

$$Y_\mathrm{out} = Y_{22} - \frac{Y_{12}^2}{Y_{11} + Y_\mathrm{Lo}}, \tag{3}$$

where Y_Lo is the total admittance of the load and receiver compensation seen from the capacitive coupler.

The input power can be expressed as

$$P_\mathrm{in} = |u_1|^2 \,\mathrm{Re}(Y_\mathrm{in}) = \frac{|u_\mathrm{s}|^2 R_0}{(R_0 + R_\mathrm{s})^2}, \tag{4}$$

where R_0 represents the load, the dielectric losses in the seawater, and the parasitic losses in the compensation circuits seen by the source. Using (4), the normalized input voltage of the CPT two-port network can be written as

$$\left|\frac{u_1}{u_\mathrm{s}}\right|^2 = \frac{1}{\mathrm{Re}\,(Y_\mathrm{in})} \frac{R_0}{(R_0 + R_\mathrm{s})^2} \tag{5}$$

The voltage gain across the network is

$$\left|\frac{u_2}{u_1}\right|^2 = \left|\frac{Y_{12}}{Y_{22} + Y_\mathrm{out}}\right|^2, \tag{6}$$

From (5) and (6), the normalized output voltage of the network can be expressed

$$\left|\frac{u_2}{u_\mathrm{s}}\right|^2 = \frac{1}{\mathrm{Re}\,(Y_\mathrm{in})} \frac{R_0}{(R_0 + R_\mathrm{s})^2} \left|\frac{Y_{12}}{Y_{22} + Y_\mathrm{out}}\right|^2, \tag{7}$$

Using (7), the efficiency of the CPT considering the source losses can be express

$$\eta = \frac{R_0}{R_0 + R_\mathrm{s}} \frac{\mathrm{Re}\,(Y_\mathrm{out})}{\mathrm{Re}\,(Y_\mathrm{in})} \left|\frac{Y_{12}}{Y_{22} + Y_\mathrm{out}}\right|^2, \tag{8}$$

Defining the following two parameters for the convenience of mathematical symbols:

$$\psi^2 = \frac{g_{12}^2}{g_{11}\, g_{22}} \tag{9a}$$

$$\chi^2 = \frac{b_{12}^2}{g_{11}\, g_{22}}, \tag{9b}$$

where g_{12} is the conductance, b_{12} is the susceptance, ψ represents the ratio between the coupling conductance and the self-conductance, and χ is equivalent to the multiplication of the quality factor and the coefficient of coupling (i.e., $\chi \approx k\,Q$).

The maximum efficiency is achieved when $\partial\eta/\partial g_\mathrm{out} = 0$ and $\partial\eta/\partial b_\mathrm{out} = 0$. First, $\partial\eta/\partial b_\mathrm{out} = 0$ is solved to optain

$$b_\mathrm{out} = g_2\,(\psi\,\chi) - b_2, \tag{10}$$

Substituting the value for (10) into $\partial\eta/\partial g_\mathrm{out} = 0$ gives

$$g_\mathrm{out} = g_2\,\sqrt{(\,1 - \psi^2\,)\,(\,1 + \chi^2\,)} \tag{11}$$

Then substituting both (10) and (10) into (8) gives

$$\eta_{max} = \frac{1}{1+a} \frac{\psi^2 + \chi^2}{\left(1 + \sqrt{(\,1 - \psi^2\,)\,(\,1 + \chi^2\,)}\right)^2 + (\psi\,\chi)^2}, \tag{12}$$

where $a = R_\mathrm{s}/R_0$ normalized source resistance to the overall resistance of the CPT system seen by the source. The first term in (12) represents the efficiency of the source and the compensation circuit on the transmitter side. The second term represents the maximum available efficiency of the capacitive coupling network similar to the one reported in [14].

If the parameter a is unity (i.e., $R_\mathrm{s} = R_0$), then maximum available power is achieved at 50% of maximum system efficiency similar to the solution in [14]. For a lossless medium, such as in an air-gapped CPT system, the (12) become

$$\eta^*_{max} = \frac{1}{1+a} \frac{\chi^2}{\left(1 + \sqrt{(\,1 + \chi^2\,)}\right)^2}, \tag{13}$$

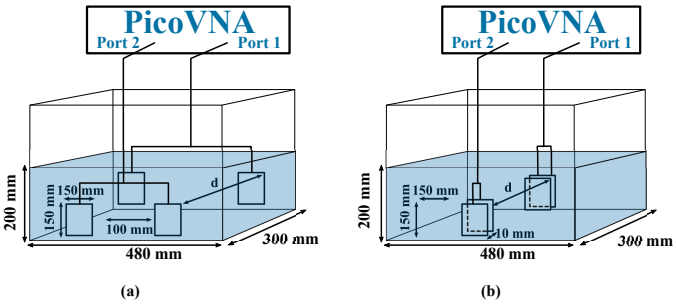

Fig. 2. The test setups: (a) Horizontal four plates configuration. (b) Vertical four plates configuration.

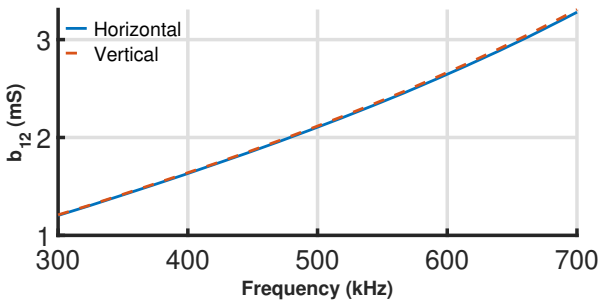

Fig. 3. The coupling susceptance under seawater for horizontal and vertical configurations.

Compared maximum efficiency of the lossless CPT system reported in [15], then χ represents the kQ product as mentioned previously in this section.

III. Experimental Results

Four 150 $\times$ 150 $\times$ 30 mm aluminum plates are used as capacitive couplers. The plates are insulated from water using a plastic lamination pouch and submerged in a container filled with 480 $\times$ 300 $\times$ 200 mm seawater that is collected from the local harbor. Using a Pico Vector Network Analyzer, the underwater admittance is measured at a distance (d) 300 mm for both horizontal and vertical configurations, as illustrated in Fig 2.

Fig. 3 shows the susceptance underwater as a function of frequency. The susceptances are linearly proportional to the frequency for horizontal and vertical configurations. The slopes of the lines are proportional to the coupling capacitance underwater. The coupling capacitance underwater is constant for both configurations over the frequency range.

Similarly, Fig. 4 presents the conductances underwater as a function of frequency. The conductances are ten times lower than the susceptances at the frequency ranges. The increase in the conductances with the increase of the frequency is attributed to the parasitic conductances of the wires that connect the plates to the VNA cables. Operating at low-frequency ranges reduces the conductive coupling under seawater, enhancing overall efficiency. The conductive coupling g_{12} of the vertical configuration has higher values than the horizontal one. Although the overall effective area of the horizontal configuration is higher than the vertical one, the cross-coupling between the plates in the horizontal configuration reduces the conductive coupling parameter.

The changing of the parameter ψ^2 with the frequency for horizontal and vertical configurations is shown in Fig. 5. As the conductive coupling g_{12} values of the vertical configuration are higher than the horizontal one, the vertical configuration has higher ψ^2 values. Fig. 6 shows that the parameter χ^2 increases with the decrease of the frequency for horizontal and vertical configurations. Although both the coupling susceptance and conductances increase with the increase of the frequency, the rate of the increase in the conductive parameters in the denominator in (9b) is faster than the increase in the

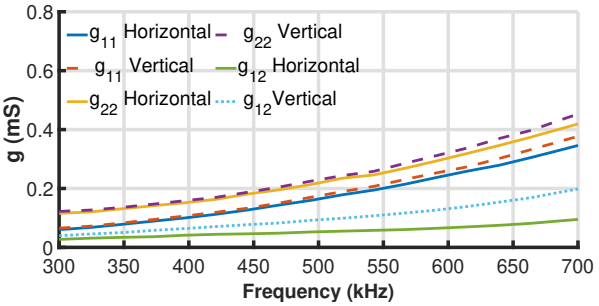

Fig. 4. The conductance of the under seawater coupling.

numerator, making the parameter χ^2 linearly decrease with the increase of the frequency.

Using the relationship in (12), Fig. 7 shows the efficiency of the underwater capacitive coupling over a frequency range 300 kHz to 700 kHz. The underwater couplers have higher efficiency at lower frequency ranges. Although the vertical configuration has higher values of the parameter ψ^2 than the horizontal one, both vertical and horizontal configurations have very close values of efficiency. This is attributed to the parameter χ^2, which is the key parameter to achieve highly efficient coupling at frequency range 300 kHz to 700 kHz, as the coupling conductivity is very low. As the χ asymptotically approaches infinity, the efficiency approaches 100% according to (12).

For experimental convenience, the vertical configuration

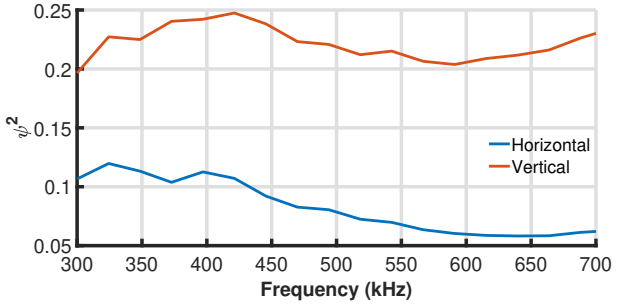

Fig. 5. The ψ of underwater capacitive coupling plates.

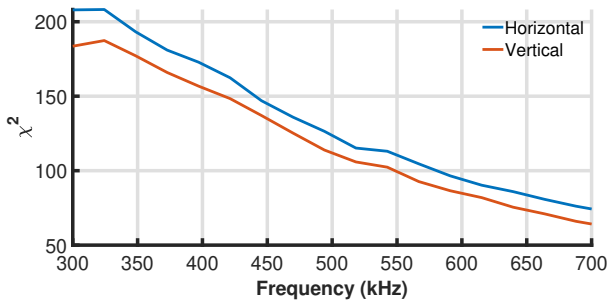

Fig. 6. The χ of underwater capacitive coupling plates.

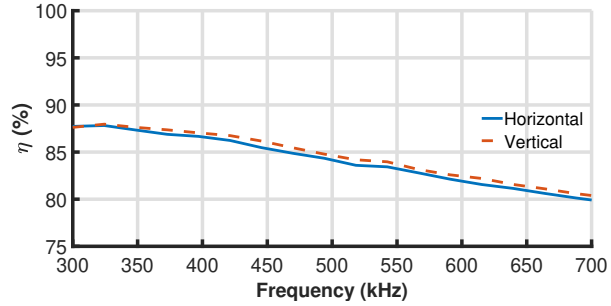

Fig. 7. The efficiency of underwater capacitive coupling plates.

will be further examined. Series compensation circuits are used. A GaN bridge inverter (Infineon EVAL1EDFG1HBGAN [16]) inverts the dc voltage into square-waveform, which is modeled as a square-wave voltage source in Fig. 1. Four Schottky diodes (C6D04065A [17]) are used to build a diode bridge that rectifies the ac transmitted power to dc. The overall CPT system configuration is illustrated in Fig. 8. PA2203A IntegraVision Power Analyzer is used to measure the output power and the dc-dc efficiency of the system.

The effect of the separation distance on the transmitted power and overall system efficiency is examined at 409 kHz and 48 Vdc input voltage. Fig. 9 shows the change in the output power and the overall efficiency of the system with the change in the separation distance. The output power and efficiency are not changing significantly with the changing of the separation distance between the transmitter and receiver couplers. When the separation distance increase from 50 mm to 500 mm, the efficiency increases from 43.5% to 44.7% while the output power decreases from about 30 W to 27 W. The enhancement in the efficiency is attributed to the decrease of the coupling conductance, and hence the parameter χ^2, with the increase of the separation distance as explained in [18].

Similarly, the effect of the operating frequency on the transmitted power and overall system efficiency is examined at the frequency ranges about 200 kHz to 700 kHz. Fig. 10 shows the change in the output power and the overall efficiency of the system with the change in the operating frequency. The maximum efficiency is 57.3% is achieved at 337 kHz, while the maximum output power is about 48 W at 516 kHz operating frequency. Fig. 11 shows the calculated efficiencies

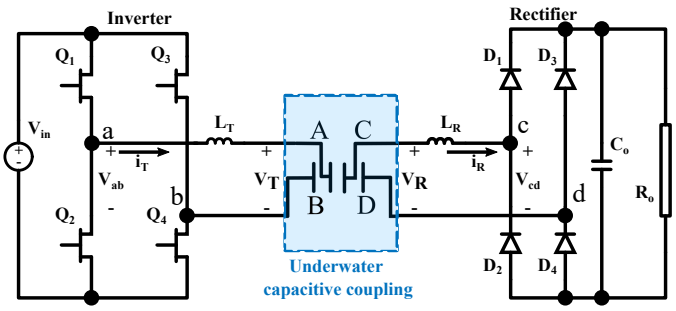

Fig. 8. The converter configuration of underwater CPT system.

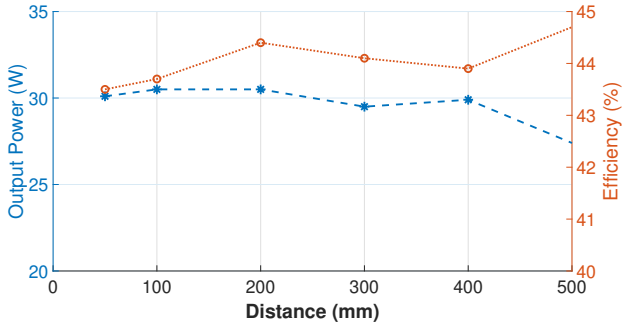

Fig. 9. The changing of the output power and overall system efficiency with changing the separation distance.

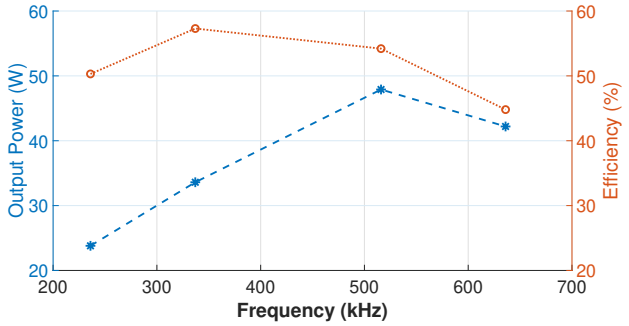

Fig. 10. The changing of the output power and overall system efficiency with changing of the operating frequency.

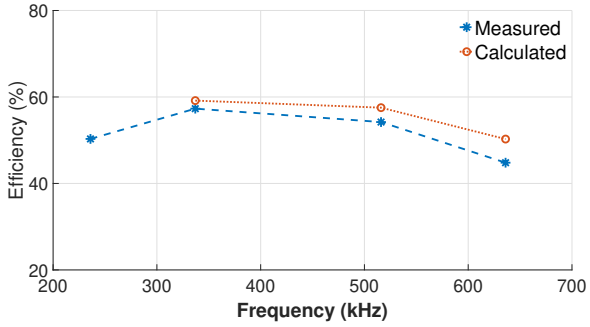

Fig. 11. The calculated and measured efficiencies with the change of the frequencies.

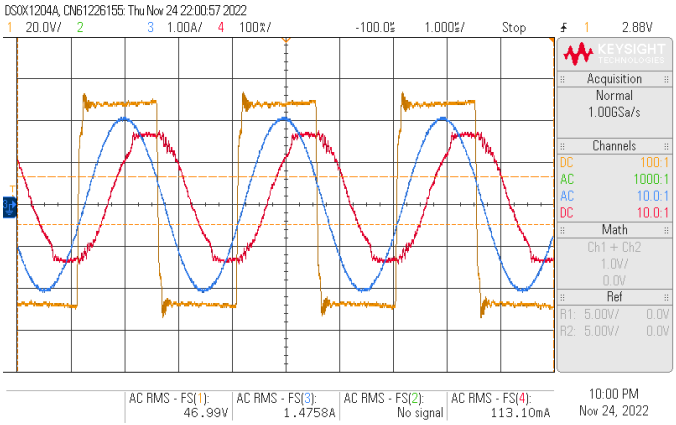

Fig. 12. The waveforms at maximum efficiency: the output voltage of the inverter V_{ab} (yellow), the transmitter current i_{T} (blue), and the receiver current i_{R} (red).

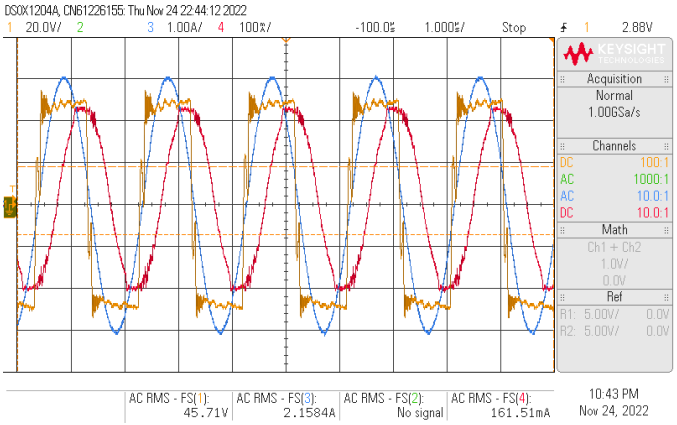

Fig. 13. The waveforms at maximum power: the output voltage of the inverter V_{ab} (yellow), the transmitter current i_{T} (blue), and the receiver current i_{R} (red).

from (12) and measured values under the change of the operating frequencies. The maximum ON-resistors of enhancement mode transistors and the losses in the transmitter inductor are considered as the source resistance R_{s}, as mentioned previously in section and shown in Fig.1. However, the internal resistance of the dc source is not considered in the calculated efficiencies, which might explain the difference between the calculated and measured values.

Fig. 12 and 13 shows the inverter output voltage and the transmitter and receiver current waveforms at maximum efficiency and maximum power, respectively. In both cases, the phase shift between the transmitter and receiver currents is about 90 degrees which result in zero transmitted reactive power [19]. Fig. 12 shows that the transmitter current is slightly lagging behind the output voltage of the inverter, which helps to achieve the zero voltage switching condition for the switches. In contrast, Fig. 13 shows that the transmitter current is in phase with the output voltage of the inverter, which means the zero phase angle condition is achieved, and hence a minimum VA rating of power supply is required. However, as the transmitter and receiver currents are high, there will be more losses in the system.

Table I summarizes a comparison of the performances of the designed system with the recently proposed underwater CPT systems. The papers [12], [13] investigate high-frequency operating CPT systems under fresh and seawater, respectively. They managed to transfer hundreds of watts over a separation distance of $20\,\mathrm{mm}$, which is short enough to achieve high ac-ac efficiency of higher than 90%. However, operating at high-frequency to transfer high power might face practical challenges.

The researchers in [20] transmitted $100\,\mathrm{W}$ at $500\,\mathrm{kHz}$ operating frequency and separation distance of $400\,\mathrm{mm}$. As the operation conditions are not far from this work, the efficiency that they achieved is 50%. However, the input voltage that they used is $100\,\mathrm{V}$, increasing the input voltage results in increasing the resistance R_{o}. Thus, operating the system proposed in this paper at $100\,\mathrm{V}$ is expected to have better efficiency and higher power. Another approach to improve the efficiency further is using another type of compensation circuit (i.e., large R_{o} hence no reflected power) and reactive compensation for underwater CPT transfer system.

Finally, paper [21] transferred $100\,\mathrm{W}$ at $625\,\mathrm{kHz}$ operating frequency and separation distance of $150\,\mathrm{mm}$ using more complex compensation circuits. However, the paper investigated the underwater effect by placing a seawater bag between air-gapped plates, which neglects the fringing effects and the cross-coupling effects between the plates. Thus, the reported results will be different if the capacitive couplers are submerged in water.

IV. Conclusion

This paper investigated CPT submerged in seawater for maritime charging applications. It proposed and validated a mathematical model to calculate the maximum achievable efficiency of the CPT system considering the dielectric losses of the medium. Moreover, the effect of changing separation distance and switching frequency on the transmitted power and the overall efficiency is examined using series compensation. While the distance has almost little effect on the power transfer and efficiency, the operating frequency considerably affects the performance of the system. The paper tests series compensation circuit to transfer $48\,\mathrm{W}$ at $500\,\mathrm{mm}$, $48\,\mathrm{V}$ input voltage, $516\,\mathrm{kHz}$, and 54%. Operating the system at low frequencies can improve the overall efficiency while limiting the transferred power. Different compensation circuits are required to achieve a better solution to enhance efficiency and power transferability.

References

[1] D. F. Campos, A. Matos, and A. M. Pinto, "Modular multi-domain aware autonomous surface vehicle for inspection," *IEEE Access*, vol. 10, pp. 113 355–113 375, 2022.

[2] G. Shao, Y. Ma, R. Malekian, X. Yan, and Z. Li, "A novel cooperative platform design for coupled usv–uav systems," *IEEE Transactions on Industrial Informatics*, vol. 15, no. 9, pp. 4913–4922, 2019.

TABLE I
COMPARISON OF THE RECENTLY PROPOSED UNDERWATER CPT SYSTEMS.

Ref.	**Compensation**	**Frequency** (MHz)	**Distance** (mm)	**Power** (W)	**Efficiency** (%)
[13]	Series-series	6.78	20	1000	94.5[1]
[12]	Series-series	107.7	20	400	90[1]
[20]	Series-series	0.5	400	100	50
[21]	LCLC-LCLCL	0.625	150	100	80.2
This work	Series-series	0.516	500	48	54

[1]ac-ac efficiency

[3] Y. Zhao, X. Qi, Y. Ma, Z. Li, R. Malekian, and M. A. Sotelo, "Path following optimization for an underactuated usv using smoothly-convergent deep reinforcement learning," *IEEE Transactions on Intelligent Transportation Systems*, vol. 22, no. 10, pp. 6208–6220, 2021.

[4] C. R. Teeneti, T. T. Truscott, D. N. Beal, and Z. Pantic, "Review of wireless charging systems for autonomous underwater vehicles," *IEEE Journal of Oceanic Engineering*, vol. 46, no. 1, pp. 68–87, 2021.

[5] K. Xue, C. Ren, X. Ji, and H. A. Qian, "Design, modeling and implementation of a projectile-based mechanism for usvs charging tasks," *IEEE Robotics and Automation Letters*, pp. 1–1, 2022.

[6] B. Allen, T. Austin, N. Forrester, R. Goldsborough, A. Kukulya, G. Packard, M. Purcell, and R. Stokey, "Autonomous docking demonstrations with enhanced remus technology," in *OCEANS 2006*, 2006, pp. 1–6.

[7] C. R. Teeneti, T. T. Truscott, D. N. Beal, and Z. Pantic, "Review of wireless charging systems for autonomous underwater vehicles," *IEEE Journal of Oceanic Engineering*, vol. 46, no. 1, pp. 68–87, 2021.

[8] J. Kim, K. Kim, H. Kim, D. Kim, J. Park, and S. Ahn, "An efficient modeling for underwater wireless power transfer using z-parameters," *IEEE Transactions on Electromagnetic Compatibility*, vol. 61, no. 6, pp. 2006–2014, 2019.

[9] C. Cai, Y. Zhang, S. Wu, J. Liu, Z. Zhang, and L. Jiang, "A circumferential coupled dipole-coil magnetic coupler for autonomous underwater vehicles wireless charging applications," *IEEE Access*, vol. 8, pp. 65 432–65 442, 2020.

[10] Z. Yan, K. Zhang, L. Qiao, Y. Hu, and B. Song, "A multiload wireless power transfer system with concentrated magnetic field for auv cluster system," *IEEE Transactions on Industry Applications*, vol. 58, no. 1, pp. 1307–1314, 2022.

[11] Y. Zeng, C. Lu, R. Liu, X. He, C. Rong, and M. Liu, "Wireless power and data transfer system using multidirectional magnetic coupler for swarm auvs," *IEEE Transactions on Power Electronics*, vol. 38, no. 2, pp. 1440–1444, 2023.

[12] M. Tamura, Y. Naka, K. Murai, and T. Nakata, "Design of a capacitive wireless power transfer system for operation in fresh water," *IEEE Transactions on Microwave Theory and Techniques*, vol. 66, no. 12, pp. 5873–5884, 2018.

[13] M. Tamura, K. Murai, and M. Matsumoto, "Design of conductive coupler for underwater wireless power and data transfer," *IEEE Transactions on Microwave Theory and Techniques*, vol. 69, no. 1, pp. 1161–1175, 2021.

[14] H. Mahdi, B. Hoff, and T. Østrem, "Optimal solutions for underwater capacitive power transfer," *Sensors*, vol. 21, no. 24, p. 8233, 2021.

[15] Y. Wang, H. Zhang, and F. Lu, "Review, analysis, and design of four basic cpt topologies and the application of high-order compensation networks," *IEEE Transactions on Power Electronics*, vol. 37, no. 5, pp. 6181–6193, 2022.

[16] CoolGaN, "High-frequency half-bridge evaluation board featuring EiceDRIVER™ GaN," May 2022, [Online; accessed 25. May. 2022]. [Online]. Available: https://www.infineon.com/cms/en/product/evaluation-boards/eval_1edf_g1b_hb_gan/

[17] Wolfspeed, "Silicon Carbide Schottky Diode," May 2022, [Online; accessed 25. May. 2022]. [Online]. Available: https://assets.wolfspeed.com/uploads/2020/12/C6D04065A.pdf

[18] H. Mahdi, B. Hoff, P. G. Ellingsen, and T. Østrem, "Conformal transformation analysis of capacitive wireless charging," *IEEE Access*, vol. 10, pp. 105 621–105 630, 2022.

[19] F. Lu, H. Zhang, and C. Mi, "A two-plate capacitive wireless power transfer system for electric vehicle charging applications," *IEEE Transactions on Power Electronics*, vol. 33, no. 2, pp. 964–969, 2018.

[20] L. Yang, Y. Zhang, X. Li, J. Jian, Z. Wang, J. Huang, L. Ma, and X. Tong, "Analysis and design of four-plate capacitive wireless power transfer system for undersea applications," *CES Transactions on Electrical Machines and Systems*, vol. 5, no. 3, pp. 202–211, 2021.

[21] L. Yang, M. Ju, and B. Zhang, "Bidirectional undersea capacitive wireless power transfer system," *IEEE Access*, vol. 7, pp. 121 046–121 054, 2019.